Macromolecules

ARTICLE

pubs.acs.org/Macromolecules

Water-Soluble Iridium(III)-Containing Conjugated Polyelectrolytes with Weakened Energy Transfer Properties for Multicolor Protein Sensing Applications

Pengfei Sun,[†] Xiaomei Lu,[†] Quli Fan,[*,†] Zhiyong Zhang,[†] Wenli Song,[†] Bo Li,[†] Ling Huang,[‡] Jinwen Peng,[§] and Wei Huang[*,†]

[†]Key Laboratory for Organic Electronics & Information Displays (KLOEID) and Institute of Advanced Materials (IAM), Nanjing University of Posts & Telecommunications (NUPT), 9 Wenyuan Road, Nanjing 210046, Jiangsu, China

[‡]School of Chemical and Biomedical Engineering, Nanyang Technological University, Singapore 637457

[§]College of Material Science and Engineering, Guilin University of Technology (GUT), 12 Jiangan Road Guilin 541004, Guangxi, China

Supporting Information

ABSTRACT: Cationic conjugated polyelectrolytes (CPEs) containing an iridium complex ($(ppy)_2Ir(FlPy)$) as the energy acceptor were synthesized via Suzuki coupling reaction. The polymer with 12 mol % $(ppy)_2Ir(FlPy)$ (**P4**) shows efficient intrinsic fluorescence resonance energy transfer (FRET) in aqueous solution due to the solubility-limitation-caused polymer aggregation. Thus, at a relatively high concentration, **P4** emits dual-emissive red phosphorescence upon donor excitation. Investigation of the emission responses of **P4** toward proteins reveals a unique weakened FRET process from the main segments (donor) to the $(ppy)_2Ir(FlPy)$ units (acceptor) in the presence of histone instead of other proteins. With such a selective weakened FRET process, the emission color of **P4** solution turns from red into lilac only in the presence of histone, allowing for visual discrimination of histone. Moreover, the linearity of this weakened FRET of **P4** also enables effective quantification of histone with a limit of detection of 0.06 μM. This study thus provides a new design concept to take full advantage of polymer solubility limitation for CPE-based multicolor visual sensing.

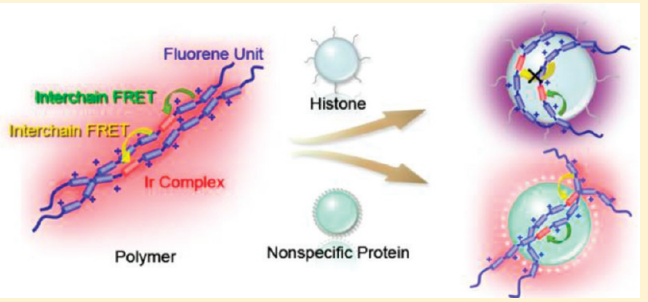

INTRODUCTION

Fluorescent materials with protein sensing capability are of scientific significance and economic interest because of their vial applications ranging from proteomics, to medical diagnostics, and to pathogen detection.[1] Owing to their higher structural complexity and environmental sensitivity relative to other biomolecules, effective protein sensing materials should not only bear appropriate receptors for efficient binding with target proteins but also possess perturbable functionalities for sensitive transduction of recognition events.[2] Conjugated polyelectrolytes (CPEs) composed of π-conjugated fluorescent backbones with amenable water-soluble side chains well fulfill these requirements.[3] For instance, the electron-delocalized backbones of CPEs facilitate rapid intrachain and interchain exciton migrations, bringing in amplified signals and improved sensitivity as compared to small fluorophores,[4] while their numerous charged side chains along fluorescent backbones orchestrate their electrostatic behaviors in aqueous media, resulting in efficient multiple interactions with proteins. CPEs thus hold great promise in protein sensing.[5]

Fluorescent quenching,[6] colorimetric,[7] and fluorescence resonance energy transfer (FRET) properties[8] of CPEs have been utilized for protein detection. In comparison with fluorescence quenching and colorimetric assays, FRET-based sensing strategy has the unique advantage of dual-channel signal collection, consequently leading to reduced possibility of false-positive signals.[9] Array-based and specific proteins assays have been developed by taking advantage of distance-sensitive FRET between CPEs and dye-labeled probes. Recently, label-free FRET protein assays have also been developed using CPEs with energy donor−acceptor architecture.[10] The working mechanism relies on the hypothesis that three-dimensional interchain FRET is more efficient than one-dimensional intrachain FRET due to the stronger electronic coupling of the former.[11] Upon CPE/protein complexation, polymer aggregation occurs to favor FRET from the donor segments to the acceptor units, giving to fluorescent color variation. The efficiency of such aggregation-enhanced FRET is strongly dependent on the nature of proteins such as net charges, inorganic components, and hydrophobicity, consequently making protein discrimination possible.

Despite the usability of aggregation-enhanced FRET for protein sensing, CPEs with energy donor−acceptor architecture

Received: July 14, 2011
Revised: September 13, 2011
Published: October 24, 2011

dx.doi.org/10.1021/ma201614z | *Macromolecules* 2011, 44, 8763–8770

usually suffer from undesired FRET prior to analyte addition, giving rise to low signal-to-noise ratios and narrow detection ranges.[12] These drawbacks originate from the hydrophobic nature of aromatic backbones of CPEs that greatly limits their water solubility and subsequently induces self-aggregation in aqueous solution.[13] Although the undesirable self-aggregation-induced FRET could be possibly minimized by attaching highly water-soluble bulky side chains such as peripheral charged amino groups[14] and cationic poly(ethylene glycol),[15] interchain FRET could be simultaneously inhabited, leading to compromised sensitivity. As such, other sensing concept that makes full use of self-aggregation-induced FRET of CPEs remains unrevealed and greatly challenging for protein sensing.

In this contribution, we report for the first time that CPEs with donor−acceptor architecture can show weakened FRET responses toward proteins. As shown in Scheme 1, these cationic CPEs (**P3** and **P4**) have a blue-fluorescent polyfluorene (PF) backbone incorporated with different amounts of red-phosphorescence iridium(III) complex as the energy acceptor. Iridium(III) complex is chosen herein considering its efficient FRET with PF as demonstrated in our previous reports.[16] In addition, the relatively higher hydrophobicity of iridium(III) complex as compared to organic units such as 2,1,3-benzothiadiazole (BT) is also beneficial to more efficient self-aggregation-induced FRET. **P4** with 12 mol % acceptor shows a stronger FRET-induced acceptor emission than **P3** with 6 mol % acceptor does. Investigation on the optical responses of **P4** toward different proteins reveals that weakened FRET occurs only in the presence of histone, leading to the emission color variation from red to lilac for visual detection of histone.

Scheme 1. Chemical Structures of P3 and P4

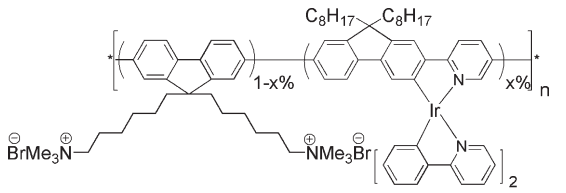

P3 X=6
P4 X=12

RESULTS AND DISCUSSION

Synthesis and Characterization. Scheme 2 shows the design of $(ppy)_2Ir(BrFlPyBr)$ iridium(III) complexes comprise two cyclometalating C^N phenylpyridine ligands and one C^N 5-bromo-2-(2-bromo-9,9′-dioctyl-9*H*-fluoren-7-yl)pyridine. The ligand material, 5-bromo-2-(2-bromo-9,9-dioctyl-9*H*-fluorene-7-yl)pyridine, was prepared by reacting 2-(4′,4′,5′,5′-tetramethyl-1′,3′,2′-dioxaborolan-2′-yl)-7-bromo-9,9-dioctylfluorene with 2,5-dibromopyridine in THF using $Pd(PPh_3)_4$ as catalyst (Scheme 2), according to a literature procedure.[17] The correct chemical structure of **2** was affirmed by NMR and GCMS. The synthetic procedure used to prepare these compound, $(ppy)_2Ir(BrFlPyBr)$, involved two steps. First, a two cyclometalating C^N phenylpyridine ligand, $[(ppy)_2IrCl]_2$, was prepared according to the Nonoyama route, by refluxing $IrCl_3 \cdot nH_2O$ with 2.2 equiv of 4-pyrazole-1-yl-benzaldehyde in a 3:1 mixture of 2-ethoxyethanol and water for 24 h.[18] $(ppy)_2Ir(BrFlPyBr)$ iridium complexes were then obtained by reaction of the chloride-bridged dimer with another C^N ligand in the presence of K_2CO_3 in *m*-cresol at 200 °C for 22 h. The complex obtained after this second step was confirmed by ^1H NMR and MALDI-TOF.

The synthesis route toward **P3** and **P4** is shown in Scheme 3. The neutral precursors (**P1** and **P2**) with 6 and 12 mol % iridium(III) complex, respectively, were synthesized via standard Suzuki coupling polymerization. Their molecular structure is confirmed by its ^1H NMR spectra. (Detailed ^1H NMR spectra of **P1** and **P2** are shown in the Supporting Information as Figure S1.) The number-average molecular weight and polydispersity are 18 900 and 2.08 for **P1** and 37 700 and 2.67 for **P2**, respectively, determined by gel-permeation chromatography (GPC) using tetrahydrofuran (THF) as the solvent and polystyrene as the standard. Quaternization of the neutral precursors by treatment of condensed trimethylamine at −78 °C provided the target CPEs (**P3** and **P4**). The chemical structures of **P3** and **P4** were also confirmed by ^1H NMR spectra. For **P3** and **P4**, comparing the relative integrals of the peak at 3.00 ppm for $-CH_2C\underline{H}_2CH_2CH_2CH_2CH_2X$ (X = Br, N $(CH_3)_3$) with that of 0.83 ppm for $-CH_2CH_2N\,(C\underline{H}_3)_3$ in the ^1H NMR spectra can be used to estimate the quaternization degrees of **P3** and **P4** which are 90% and 92%, respectively. (Detailed ^1H NMR spectra of **P3** and **P4** are shown in the Supporting Information as Figure S2.)

Scheme 2. Synthetic Scheme of the Iridium Complex

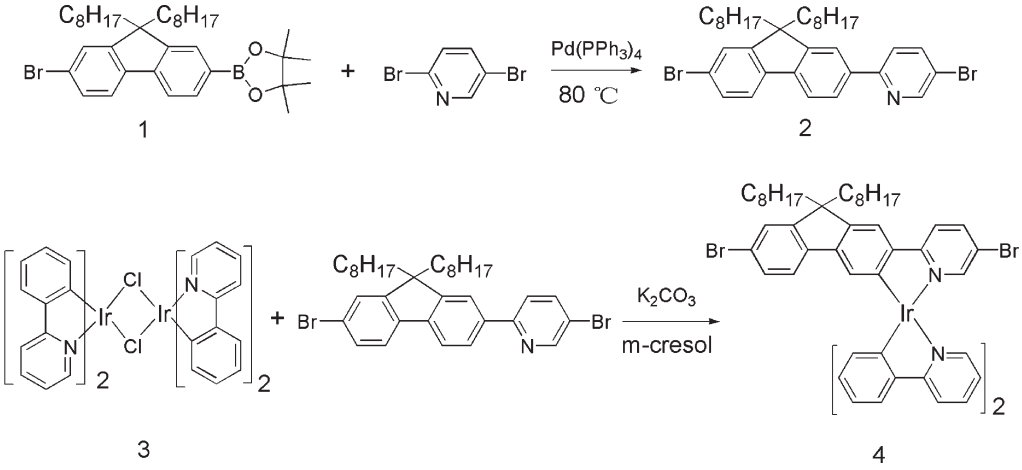

dx.doi.org/10.1021/ma201614z |*Macromolecules* 2011, 44, 8763–8770

Scheme 3. Synthetic Routes toward P3 and P4

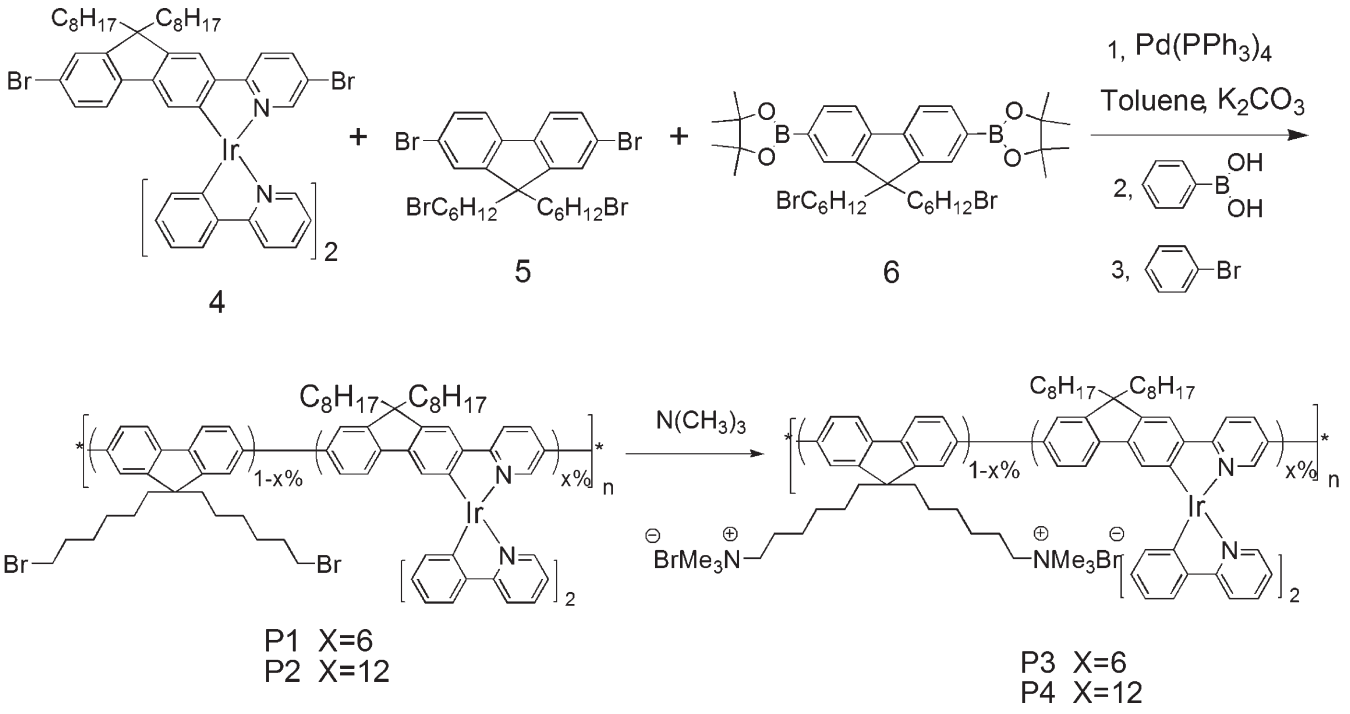

Optical Properties. The normalized UV−vis absorption spectra of **P3** and **P4** in water are shown in Figure 1a. Both polymers have an absorption maximum centered at 390 nm and an absorption band ranging from 490 to 600 nm, which are corresponding to the fluorene segments and iridium(III) complex, respectively. The photoluminescence (PL) quantum yields of **P3** and **P4** are 0.08 and 0.06 in water, respectively, measured using quinine sulfate in 0.1 M H_2SO_4 (quantum yield = 0.55) as a standard. The normalized PL spectra of both polymers in water at [RU] = 1 and 10 μM upon excitation at 380 nm are shown in Figures 1b and 1c, respectively. Regardless of the concentration, both polymers show an emission peak at 430 nm corresponding to the fluorescence of PF segments. However, the emission peak at 605 nm corresponding to the phosphorescence of iridium(III) complex only appears for **P3** at [RU] = 10 μM, while it always exists and becomes stronger with increasing concentration for **P4**. The difference in the PL spectral profiles clearly reveals that **P4** has a more efficient self-aggregation-induced FRET as compared to **P3** due to its higher acceptor concentration. Thus, **P4** is more suitable than **P3** for protein sensing. Moreover, these data also show that self-aggregation-induced FRET enhances with increasing concentration as a result of intensified polymer aggregation at elevated concentration. With such an efficient self-aggregation-induced FRET of **P4** at [RU] = 10 μM, the emission color of the polymer solution is red, making it ideal for protein sensing based on weakened FRET.

Protein Sensing. To demonstrate the protein sensing capability, the PL spectra responses of **P4** toward nine different proteins are examined at [RU] = 10 μM in phosphate buffered saline (PBS, 2 mM, pH = 7.4) upon excitation at 380 nm. The proteins include histone, α-fetoprotein (AFP), bovine serum albumin (BSA), thrombin (Thro), glucose oxidase (GOX), lysozyme (Lys), cytochrome *c* (CytC), hemoglobin (Hb), and myoglobin (Mb), which have the isoelectric point (pI) at ~11.7, 4.75, 4.8, 7.1, 4.6, 11, 10.7, 6.75, and 7.07, respectively. The PL spectra of **P4** upon addition of histone with the concentration ranging from 0 to 10 μM at intervals of 1 μM are shown in Figure 2a. With increasing [histone], the donor emission intensity at 430 nm (I_{430}) gradually increases, which is concomitant with the acceptor emission intensity decreases at 605 nm (I_{605}). The saturation occurs at [histone] = 10 μM, where the red emission no long decreases. In sharp contrast, other proteins such as AFP, BSA, Thro, GOX, and Lys slightly disturb the PL spectrum of **P4**. The PL spectra upon addition of other proteins are shown in Figure 2b-1. While in Figure 2b-2, the photoluminescence of **P4** was efficiently quenched after adding iron metallproteins such as Hb, Mb, and Cytc. This quenching phenomenon results from the formed electron transfer between the conjugated backbone and the iron complex.[19] To quantify the protein effect on the FRET of **P4**, I_{430}/I_{605} in the presence of proteins (10 μM) is summarized in Figure 2c. It can be seen that only histone can induce a significant increase in I_{430}/I_{605}, which is substantially larger than other proteins. Because of this unique histone-induced FRET-weakened process of **P4**, the emission color of the polymer solution changes from red to lilac in the presence of histone (Figure 2d), while it remains red for other proteins. As a result, visual discrimination of histone from other proteins is feasible based on **P4**. As histone is a vital protein that abounds in nucleoli and plays an indispensable role in complexation with DNA to form chromosomes,[20] this visual detection method is of potential importance for proteomics.

The selectively weakened FRET responses of **P4** should be mainly associated with the polymer/protein interactions including hydrophobic and electrostatic interactions. According to pI values, these proteins can be divided into two groups at pH = 7.4: the positively charged proteins (histone, Lys, and CytC) and the

dx.doi.org/10.1021/ma201614z |*Macromolecules* 2011, 44, 8763–8770

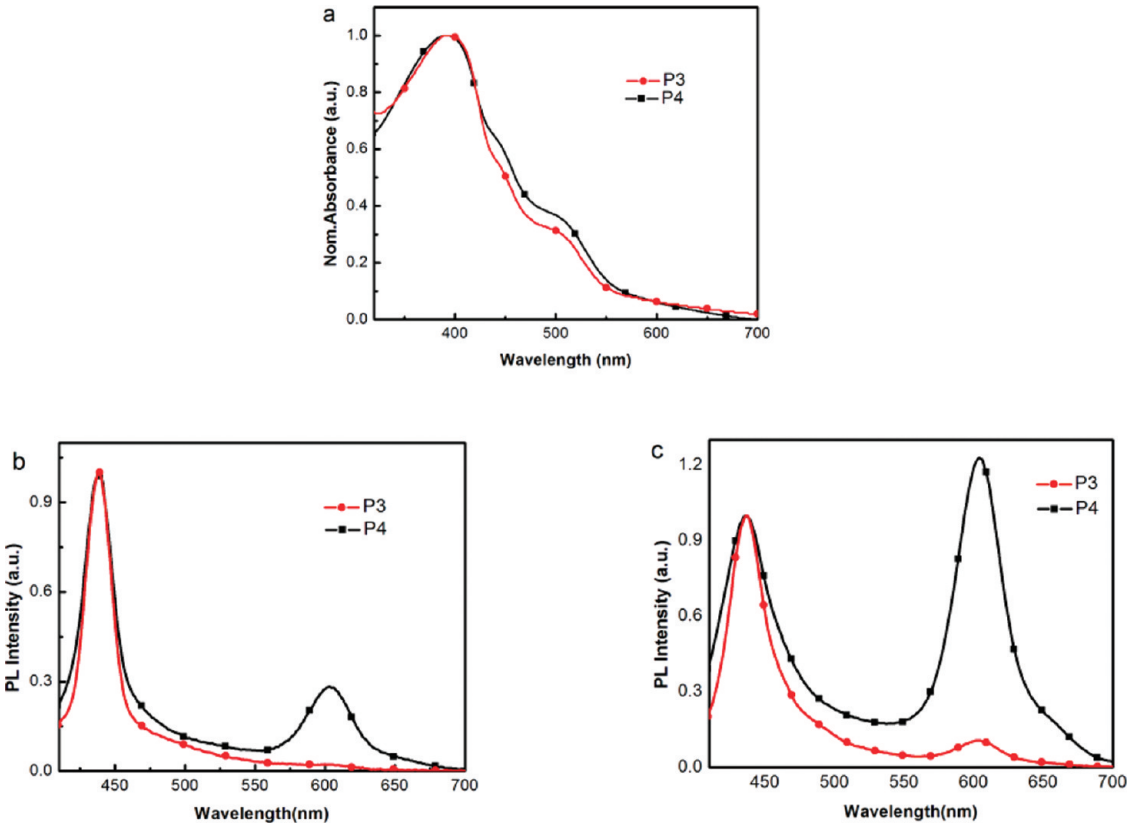

Figure 1. Normalized UV−vis absorption spectra of **P3** and **P4** in water (a) and normalized PL spectra of **P3** and **P4** at [RU] = 1 μM (b) and [RU] = 10 μ M (c) in water (excitation at 380 nm).

negative charged proteins (AFP, BSA, Thro, GOX, Hb, and Mb). Considering that **P4** is positively charged, electrostatic attraction exists for the latter group. However, addition of these oppositely charged proteins into the polymer solution does not contribute to further enhancing the FRET for **P4**, as shown in Figure 2b. This observation can be rationalized by the fact that the polymer self-aggregation forms intrinsically in aqueous solution, and thus addition of oppositely charged proteins can only interact with the large aggregates instead of single polymer chains. Under these circumstances, the interchain contacts within these polymer aggregates remain nearly the same before and after addition of these proteins, leading to slightly disturbed FRET for **P4**.

As electrostatic repulsion occurs between the positively charged polymer and the proteins, addition of these proteins should in principle also have a neglectable effect on FRET for **P4**. Although both CytC and Lys comply well with this deduction, weakened FRET is surprisingly observed for **P4** in the presence of histone. In order to further understand the effect of the electrostatic interaction of histone and **P4**, the pH dependence of the photoluminescence of the histone/**P4** complex was investigated. Considering the pI of histone is 11.7, the PL spectra responses of **P4** toward histone at pH = 3, 7, and 12 were studied, and the results are shown in Figure 3. When the pH varies from 3 to 7, the PL spectra of **P4** are nearly unchanged. When pH increases to 12, the PL intensity dramatically decreases which can be explained by the enhanced interchain aggregation.[21] It is interesting to find that after adding histone all the emission intensities at 430 nm (I_{430}) increase while the emission intensity at 605 nm (I_{605}) decreases, regardless of the pH. Such a pH-independent phenomenon clearly demonstrates that the effect of electrostatic interactions on the FRET-weakened process can be ruled out.

This unusual phenomenon clearly reflects that hydrophobic interaction between histone and polymer is stronger enough to break self-formed polymer aggregates into a certain extent. On the other hand, it is intriguing to find that when **P4** is at [RU] = 1 μM with little interchain aggregation, the change of PL intensity is not observed after adding histone. Furthermore, I_{430}/I_{605} of **P4** at [RU] = 10 μM in the presence of 10 μM histone (3.96) is nearly equal to that of **P4** at [RU] = 1 μM (3.60). This consistency further reveals that the polymer chains of **P4** in the presence of 10 μM histone stay in a nearly single-molecular state that is similar to that in dilute solution. According to the related previous study, in comparison with other proteins, histone exhibits strong hydrophobicity, and thus it can enhance the aqueous solubility of CPEs.[6a,22] Therefore, different from other proteins, histone is considered to be able to break self-formed polymer aggregates into a certain extent, minimizing the interchain FRET process and change the polymer fluorescent color.

According to the above explanation, the working mechanism for weakened FRET-based visual detection of histone using **P4** at a relatively high polymer concentration can be summarized in Scheme 4. In the absence of proteins, FRET occurs due to polymer self-aggregation induced by its poor water solubility, which leads to the dual-emissive red emission upon donor excitation. In the presence of histone, the hydrophobic interaction between the polymer and histone breaks self-aggregates and thus minimizes the interchain FRET process, ultimately giving rise to lilac emission. In contrast, other proteins cannot influence

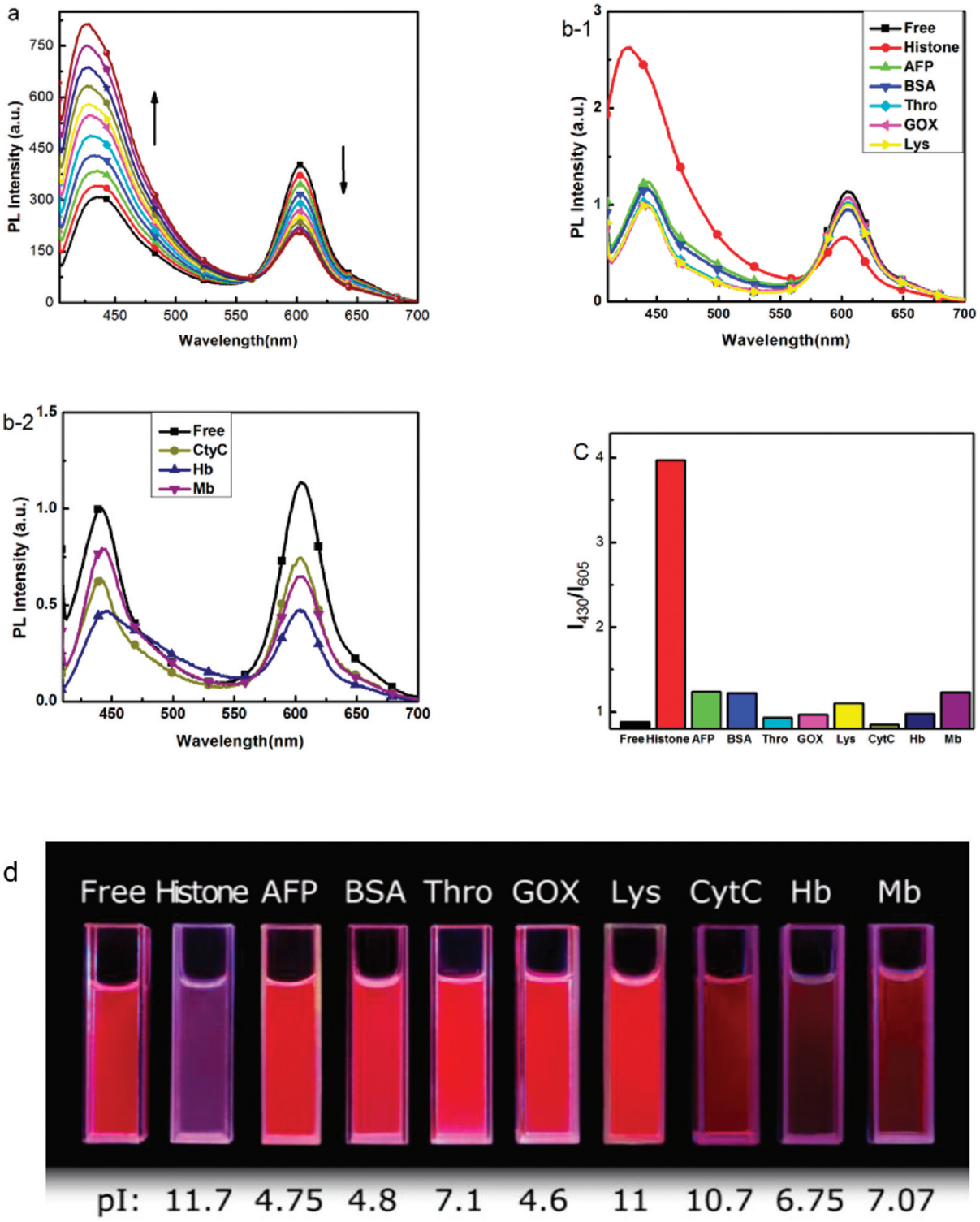

Figure 2. (a) PL spectra of **P4** in PBS (2 mM, pH = 7.4) in the absence and presence of histone with the concentration ranging from 0 to 10 μM at intervals of 1 μM. [RU] = 10 μM. Excitation at 380 nm. (b) PL spectra of **P4** in PBS (2 mM, pH = 7.4) in the absence and presence of different proteins. [P4RU] = 10 μM, and [protein] = 10 μM. Excitation at 380 nm. (c) The intensity ratio of the blue emission at 430 nm to the red emission of **P4** at 605 nm (I_{430}/I_{605}) as a function of proteins. (d) Photographs of the corresponding emissive solutions of **P4** in the presence of different proteins under UV radiation at 365 nm.

the organization of polymer aggregates, making the emission of **P4** remain in red.

Protein Quantification. To demonstrate histone quantification, changes in the PL spectra in Figure 2a are correlated with [histone] using I_{430}/I_{605} as the calibration parameter. Figure 4 shows I_{430}/I_{605} as a function of [histone] along with its linear fitting line. The original data show good overlap with the linear fitting line in the range of 0−10 μM, indicating the validity of **P4**

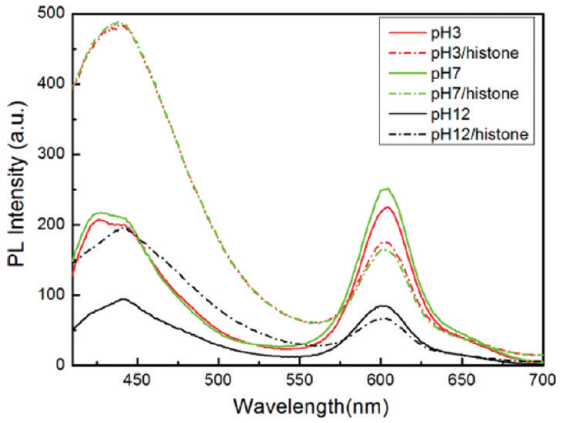

Figure 3. PL spectra of **P4** in pH = 3, 7, and 12 in the absence and presence of histone ([RU] = 10 μM) at [RU] = 10 μM. Excitation at 380 nm.

Scheme 4. Schematic Illustration of Weakened FRET-Based Visual Detection of Histone Using P4

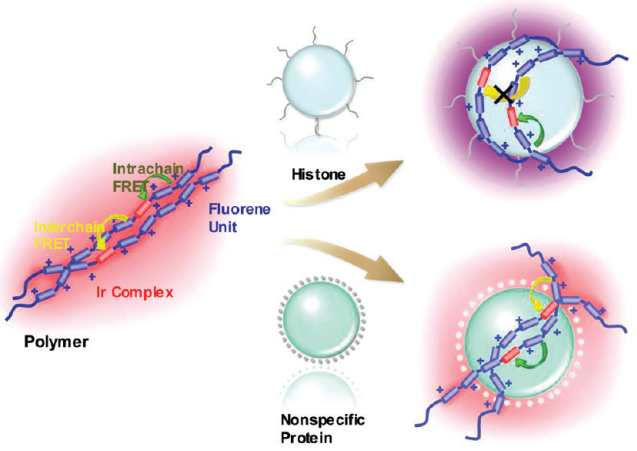

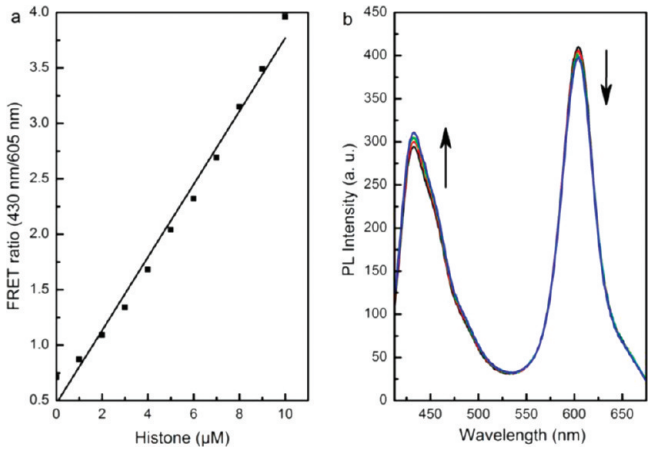

Figure 4. (a) I_{430}/I_{605} as a function of [histone] along with its linear fitting line. (b) PL spectra of **P4** in PBS (2 mM, pH = 7.4) with addition of histone with the concentration ranging from 0 to 0.18 μM at intervals of 0.06 μM. [RU] = 10 μM. Excitation at 380 nm.

in histone quantification. The limit of detection (LOD) is tested by reducing the addition amount of histone into the polymer solution. As shown in Figure 4b, addition of 0.06 μM histone into the polymer solution can still increase emission intensity at 430 nm (weakened FRET for **P4**), while further decreasing the addition amount to 0.06 μM fails to give observable changes in the PL spectrum of **P4**. Accordingly, the practical LOD for **P4** in histone quantification is determined as 0.06 μM.

CONCLUSIONS

We have designed and synthesized iridium(III) complex containing cationic CPEs with energy donor−acceptor architecture for visual protein sensing. The polymer having 12 mol % iridium(III) complex (**P4**) undergoes self-aggregation-induced FRET in aqueous solution. This self-aggregation-induced FRET process becomes stronger at elevated concentration as a result of increased polymer aggregation, which consequently leads to dual-emissive red emission upon donor excitation at 380 nm. Among nine tested proteins, only histone can effectively break the polymer aggregates and in turn induce a weakened FRET process from the main segments (donor) to the $(ppy)_2Ir(FlPy)$ units (acceptor). As such, the emission color of **P4** solution varies from red into lilac upon addition of histone, allowing for visual discrimination of histone from other four proteins by the naked eye. Moreover, the linearity of the intensity changes at donor/acceptor emission enables effective quantification of histone with a practical LOD of 0.06 μM. With these desirable features, these iridium(III) complex containing cationic CPEs hold great promise in rapid detection and quantification of histone in purified form.

In conclusion, this study has demonstrated a new generation of CPEs with energy donor−acceptor backbones that circumvent the solubility-caused limitation to possess weakened FRET for multicolor protein sensing. From the materials viewpoint, other inorganic metal complexes in addition to iridium(III) complex can be similarly incorporated into CPEs to adjust the long-wavelength emission channel. As compared to organic chromophores, utilization of metal complexes as the energy acceptor has the advantage of narrowed emission, which reduces the possibility of spectral overlap and thus potentially favors multiplex detection. As a result, this study provides a new way to develop multicolor CPEs without requiring good water solubility of the polymers and thus greatly facilitates the construction of CPE-based chemical and biological sensors.

EXPERIMENTAL SECTION

General Methods. The NMR spectra were recorded on a Bruker Ultra Shield Plus 400 MHz NMR instruments (^{1}H: 400 MHz; ^{13}C: 100 MHz). The UV−vis absorption spectra were recorded on a Shimadzu UV-3600 UV−vis−NIR spectrophotometer. Photoluminescent spectra were measured using a RF-5301PC spectrofluorophotometer equipped with a xenon lamp excitation source and a Hamamatsu (Japan) 928 PMT, using 90° angle detection for solution samples. The gel permeation chromatography (GPC) analysis of the polymers was conducted on a Shim-pack GPC-80X column with THF as the eluent at a flow rate of 1.0 mL/min at 35 °C and polystyrene as standard. The data were analyzed by using the software package provided by Shimadzu Instruments. Mass spectra were obtained on a Shimadzu laser desorption/ionization time-of-flight mass spectrometer (LDI-TOF-MASS). Regenerated cellulose dialysis tubing with 1.5 or 6.5 kDa molecular weight cutoff was used for dialysis. Freeze-drying was performed using Martin Christ ModelAlpha

1-2/LD. Photographs of the fluorescent solutions were taken using a Canon EOS 500D digital camera under a hand-held UV-lamp with λ_{max} = 365 nm. All PL and UV measurements were carried out at 24 °C.

Materials. All proteins were purchased from Sigma-Aldrich Chemical Co. and were used as received. Other chemicals were purchased from Sigma-Aldrich, Acros, and Alfa and were used as-received. THF was purified by distillation from sodium in the presence of benzophenone. Other organic solvents were used without any further purification. All reactions were performed under a nitrogen atmosphere. 2-(2-Bromo-9,9-dioctyl-9*H*-fluoren-7-yl)-4,4,5,5-tetramethyl-1,3,2-dioxaborolane (**1**) and $[(ppy)_2IrCl]_2$ (**3**) were prepared according to a literature procedure.[18] 9,9′-Bis(bromohexyl)-2,7-dibromofluorene (**5**) and 2,7-bis[9,9′-bis(6″-bromohexyl)fluorenyl]-4,4,5,5-tetramethyl[1.3.2]dioxaborolane (**6**) were synthesized according to the previous literature.[17]

Synthesis of 5-Bromo-2-(2-bromo-9,9-dioctyl-9*H*-fluoren-7-yl)pyridine (2). 2-(2-Bromo-9,9-dioctyl-9*H*-fluoren-7-yl)-4,4,5,5-tetramethyl-1,3,2-dioxaborolane (**1**) (1.188 g, 2 mmol) and 2,5- dibromopyridine (0.474 g, 2 mmol) were added to a degassed solution of THF, to which a solution of Na_2CO_3 (1 M, 2 mL) was added, together with $Pd(PPh_3)_4$ (0.069 g, 3 mol % based on dibromopyridine). The resulting mixture was refluxed at 80 °C for 48 h. The reaction flask was cooled to room temperature, and the solvent was removed. The product was extracted with chloroform (3 × 30 mL), washed with water, and dried over anhydrous magnesium sulfate. Column chromatography was used to isolate the product (silica gel, petroleum ether:CH_2Cl_2, 4:1), which was recrystallized from a mixture of methanol. Fluffy, white crystals were obtained (0.75 g, 60%). ^{1}H NMR ($CDCl_3$, 400 MHz, δ): 8.76−8.75 (s, 1H), 7.94−7.95 (d, 2H), 7.89−7.86(m, 1H), 7.75−7.73 (d, 1H), 7.70 (s, 1H), 7.60−7.57 (d, 1H), 7.47−7.46 (d, 2H), 2.0−1.9 (m, 4H), 1.2−1.0 (m, 20H), 0.79 (m, 6H), 0.56 (m, 4H). ^{13}C NMR (100 MHz, $CDCl_3$, δ): 156.03, 153.52, 151.13, 150.68, 141.38, 139.26, 130.08, 126.26, 121.39, 120.08, 55.64, 40.23, 31.75, 29.90, 29.17, 23.70, 22.57, 11.04.

Synthesis of $(ppy)_2$Ir(BrFPyBr) (4). 5-Bromo-2-(2-bromo-9,9-dioctyl-9*H*-fluoren-7-yl)pyridine (0.218 g, 0.35 mmol) and $[(ppy)_2IrCl]_2$ (**3**) (0.150 g, 0.14 mmol) were dissolved in *m*-cresol (30 mL) with K_2CO_3 (0.193 g). The reaction was carried out under a nitrogen atmosphere at 200 °C for 22 h. After cooling, NaOH (saturated, 20 mL) was added to the reaction mixture, which resulted in precipitation of the orange powder product. Column chromatography (silica gel, CH_2Cl_2: petroleum ether, 1:10) enabled isolation of the pure product as an orange powder (0.19 g, 60%). ^{1}H NMR ($CDCl_3$, 400 MHz, δ): 7.92−7.88 (t, 2H), 7.83−7.81 (d, 1H), 7.69−7.58 (m, 6H), 7.56−7.55 (d, 1H), 7.52−7.51(d, 1H), 7.49 (s, 1H), 7.34 (s, 1H), 7.24−7.27 (q, 1H), 7.15−7.13 (d, 1H), 7.07 (s, 1H), 6.9−6.7 (m, 8H), 1.92−1.85 (m, 4H), 1.26−0.96 (m, 20H), 0.82−0.78 (m, 6H), 0.68−0.59 (m, 4H). ^{13}C NMR (100 MHz, $CDCl_3$, δ): 166.68, 165.79, 160.5, 153.85, 147.8, 146.97, 143.75, 142.31, 138.4, 137.06, 136.18, 129.87, 127.7, 125.7, 124.01, 122.11, 121.64, 120.58, 118.92, 116.48, 54.51, 40.98, 31.70, 29.70, 22.52, 14.11. MS (MALDI-TOF): *m*/*z* 1125.74 (M/*z*), 501.28 (M/z − $[(ppy)_2IrCl]_2$).

General Procedure for the Synthesis of P1 and P2. 9,9′-Bis(bromohexyl)-2,7-dibromofluorene (**5**) (0.366 g, 0.5 mmol), 2,7-bis[9,9′-bis(6″-bromohexyl)fluorenyl]-4,4,5,5-tetramethyl[1.3.2]dioxaborolane (**6**) (0.242 g, 0.38 mmol), and $(ppy)_2$Ir(BrFPyBr) (**4**) (0.138 g, 0.12 mmol) were dissolved in toluene (15 mL, degassed), to which a solution of K_2CO_3 (2.6 mL, 2 M) was added, together with $Pd(PPh_3)_4$ (0.025 g). The resulting mixture was sealed in a glass vial and heated for 72 h at 85 °C in an oil bath. End-capping of the polymer was carried out as the last step in synthesis. Phenylboronic acid (0.003 g, 5 mol %) was added, and the solution was heated (85 °C, 8 h). This was followed by the addition of bromobenzene (0.004 g, 5 mol %), which was heated at 85 °C for 16 h. The solution was washed with water (three times) and dried over anhydrous magnesium sulfate. After filtration, the volume of chloroform was reduced and passed through an alumina column. The volume of the resulting solution was again reduced and precipitated in methanol (500 mL); the polymer was filtered and washed with methanol and acetone and then dried under vacuum for 24 h to afford the polymers **P1** and **P2** in 85% and 80% yields, respectively. The sample was characterized by GPC in THF using polystyrene standards to obtain a molecular weight. The number-average molecular weight and polydispersity of **P1** are 18 900 and 2.08 and of **P2** are 37 700 and 2.67, respectively.

P1. ^{1}H NMR (400 MHz, $CDCl_3$) δ (ppm): 7.85−7.36 (br, 11H), 7.16−6.6 (br, 2H), 3.52−3.26 (t, 4H), 2.14−1.72 (br, 8H), 1.52−1.18 (br, 8H), 0.82−0.78 (br, 4H) (detailed ^{1}H NMR spectrum of **P1** is presented in Figure S1).

P2. ^{1}H NMR (400 MHz, $CDCl_3$) δ (ppm): 7.85−7.36 (br, 12H), 7.16−6.6 (br, 2H), 3.32−3.26 (t, 4H), 2.29−1.97 (br, 4H,), 1.72−1.7 (br, 4H), 1.25−1.14 (br, 9H), 0.85−0.81 (br, 4H) (detailed ^{1}H NMR spectrum of **P2** is presented in Figure S1).

General Procedure for the Synthesis of P3 and P4. Condensed trimethylamine (10 mL) was added dropwise to a solution of **P2** (0.4 g) in THF (10 mL) at −78 °C. The mixture was warmed to room temperature and stirred for 24 h. The formed precipitation was dissolved by addition of methanol (10 mL). After the mixture was cooled to −78 °C, additional trimethylamine (10 mL) was added. The mixture was stirred at room temperature for 24 h. The volume of the resulting solution was reduced and precipitated in acetone (500 mL); the polymer was filtered and washed with acetone and then dried under vacuum for 24 h to afford the orange powders **P3** and **P4** in 70% and 76% yields, respectively.

P3. ^{1}H NMR (400 MHz, $(CD_3)_2SO$) δ (ppm): 8.4−6.8 (fluorene), 3.8−3.7 (br, 4H), 3.0−2.8 (br, 17H), 2.0−1.8 (br, 4H), 1.5−1.4 (br, 4H), 1.2−1.1 (br, 8H), 0.82 (br, 4H) (^{1}H NMR spectrum of **P3** is presented in Figure S2).

P4. ^{1}H NMR (400 MHz, $(CD_3)_2SO$) δ (ppm): 8.0−7.0 (br,17H), 3.5 (br, 4H), 2.9 (br, 18H), 2.2 (br, 4H), 1.46 (br, 4H), 1.06 (br, 8H), 0.72 (br, 4H) (^{1}H NMR spectrum of **P4** is presented in Figure S2).

■ ASSOCIATED CONTENT

Supporting Information. Figures showing ^{1}H NMR. This material is available free of charge via the Internet at http://pubs.acs.org.

■ AUTHOR INFORMATION

Corresponding Author

*E-mail iamqlfan@njupt.edu.cn, Tel +86 25 8586 6360, Fax +86 25 8586 6396 (Q.F.); e-mail wei-huang@njupt.edu.cn, Tel +86 25 8586 6008, Fax +86 25 8586 6999 (W.H.).

■ ACKNOWLEDGMENT

This work was financially supported by the National Basic Research Program of China under Grant 2009CB930600, the National Natural Science Foundation of China under Grants 20874048, 51173080, and 21104033, the Program for New Century Excellent Talents in University under Grant NCET-10-0179, and Specialized Research Fund for the Doctoral Program of Higher Education under Grants 20093223110003 and NY211003.

■ REFERENCES

(1) (a) Kodadek, T. *Chem. Biol.* **2001**, *8*, 105–115. (b) Feng, X. L.; Liu, L. B.; Wang, S.; Zhu, D. B. *Chem. Soc. Rev.* **2010**, *39*, 2411–2419. (c) Li, K.; Liu, B. *Polym. Chem.* **2010**, *1*, 252–259.

(2) (a) Wright, A. T.; Anslyn, E. V. *Chem. Soc. Rev.* **2006**, *35*, 14–28. (b) Duan, X. R.; Liu, L. B.; Feng, F. D.; Wang, S. *Acc. Chem. Res.* **2010**, *43*, 260–270.

(3) (a) Thomas, S. W., III; Joly, G. D.; Swager, T. M. *Chem. Rev.* **2007**, *107*, 1339–1380. (b) Herland, A.; Inganäs, O. *Macromol. Rapid Commun.* **2007**, *28*, 1703–1713. (c) Nilsson, K. P. R.; Hammarström, P. *Adv. Mater.* **2008**, *20*, 2639–2645. (d) Feng, F. D.; He, F.; An, L. L.; Wang, S.; Li, Y. L.; Zhu, D. B. *Adv. Mater.* **2008**, *20*, 2959–2964. (e) Jiang, H.; Taranekar, P.; Reynolds, J. R.; Schanze, K. *Angew. Chem., Int. Ed.* **2009**, *48*, 4300–4316.

(4) (a) Swager, T. M. *Acc. Chem. Res.* **1998**, *31*, 201–207. (b) Liu, B.; Bazan, G. C. *Chem. Mater.* **2004**, *16*, 4467–4476. (c) Bazan, G. C. *J. Org. Chem.* **2007**, *72*, 8615–8635. (d) Pu, K. Y.; Liu, B. *Biosens. Bioelectron.* **2009**, *24*, 1067–1073.

(5) (a) Durate, A.; Pu, K. Y.; Liu, B.; Bazan, G. C. *Chem. Mater.* **2011**, *23*, 501–515. (b) Lee, K.; Povlich, L. K.; Kim, J. *Analyst.* **2010**, *135*, 2179–2189.

(6) (a) Kim, I. B.; Dunkhorst, A.; Bunz, U. H. F. *Langmuir* **2005**, *21*, 7985–7989. (b) Miranda, O. R.; You, C. C.; Phillips, R.; Kim, I. B.; Ghosh, P. S.; Bunz, U. H. F.; Rotello, V. M. *J. Am. Chem. Soc.* **2007**, *129*, 9856–9857.

(7) (a) Ho, H. A.; Leclerc, M. *J. Am. Chem. Soc.* **2004**, *126*, 1384–1387. (b) Béra Abérem, M.; Najari, A.; Ho, H. A.; Gravel, J. F.; Nobert, P.; Boudreau, D.; Leclerc, M. *Adv. Mater.* **2006**, *18*, 2703–2707. (c) Ho, H. A.; Najari, A.; Leclerc, M. *Acc. Chem. Res.* **2008**, *41*, 168–178.

(8) (a) Li, H. P.; Bazan, G. C. *Adv. Mater.* **2009**, *21*, 964–967. (b) Wang, J.; Liu, B. *Chem. Commun.* **2009**, *45*, 2284–2286. (c) Feng, F. D.; Liu, L. B.; Yang, Q. O.; Wang, S. *Macromol. Rapid Commun.* **2010**, *31*, 1405–1421.

(9) (a) Fan, C. H.; Plaxco, K. W.; Heeger, A. J. *Trends Biotechnol.* **2005**, *23*, 186–192. (b) Pu, K. Y.; Liu, B. *Adv. Funct. Mater.* **2009**, *19*, 1371–1378. (c) Pu, K. Y.; Li, K.; Liu, B. *Adv. Mater.* **2010**, *22*, 643–646.

(10) (a) Pu, K. Y.; Liu, B. *Macromolecules* **2008**, *41*, 6636–6640. (b) Yu, D.; Zhang, Y.; Liu, B. *Macromolecules* **2008**, *41*, 4003–4011. (c) Pu, K. Y.; Zhan, R. Y.; Liu, B. *Chem. Commun.* **2010**, *46*, 1470–1472. (d) Shi, J. B.; Cai, L. P.; Pu, K. Y.; Liu, B. *Chem.—Asian J.* **2010**, *5*, 301–308. (e) Pu, K. Y.; Shi, J. B.; Wang, L. H.; Cai, L. P.; Wang, G.; Liu, B. *Macromolecules* **2010**, *43*, 9690–9697.

(11) Schwartz, B. J. *Annu. Rev. Phys. Chem.* **2003**, *54*, 141–172.

(12) (a) Stork, M.; Gaylord, B. S.; Heeger, A. J.; Bazan, G. C. *Adv. Mater.* **2002**, *14*, 361–366. (b) Bunz, U. H. F.; Rotello, V. M. *Angew. Chem., Int. Ed.* **2010**, *49*, 3268–3279.

(13) Tan, C.; Pinto, M. R.; Kose, M. E.; Ghiviriga, I.; Schanze, K. S. *Adv. Mater.* **2004**, *16*, 1208–1212.

(14) Zhu, B.; Han, Y.; Sun, M. H.; Bo, Z. S. *Macromolecules* **2007**, *40*, 4494–4500.

(15) Pu, K. Y.; Li, K.; Liu, B. *Adv. Funct. Mater.* **2010**, *20*, 2770–2777.

(16) (a) Liu, S. J.; Zhao, Q.; Chen, R. F.; Deng, Y.; Fan, Q. L.; Li, F. Y.; Wang, L. H.; Huang, C. H.; Huang, W. *Chem.—Eur. J.* **2006**, *12*, 4351–4361. (b) Liu, S. J.; Zhao, Q.; Chen, R. F.; Deng, Y.; Xia, Y. J.; Fan, Q. L.; Huang, C. H.; Huang., W. *J. Phys. Chem. C* **2007**, *111*, 1166–1175.

(17) Albertus, J. S.; Charlotte, K. W.; Nicholas, R. E.; John, E. D.; Clare, E. B.; Anna Köhler, R. F.; Andrew, B. H. *J. Am. Chem. Soc.* **2004**, *126*, 7041–7048.

(18) Arnold, B. T.; Bert, D. A.; Peter, I. D.; Sergey, L.; Irina, T. N. H.; Robert, B.; Mark, E. T. *J. Am. Chem. Soc.* **2003**, *125*, 7377–7387.

(19) (a) Fan, C. H.; Plaxco, K. W.; Heeger, A. J. *J. Am. Chem. Soc.* **2002**, *124*, 5642–5643. (b) Cheng, F.; Zhang, G. W.; Lu, X. M.; Huang, Y. Q.; Chen, Y.; Zhou, Y.; Fan, Q. L.; Huang, W. *Macromol. Rapid Commun.* **2006**, *27*, 799–803.

(20) Nelson, D. L.; Cox, M. M. *Lehninger Principles of Biochemistry*, 4th ed.; W.H. Freeman: New York, 2004.

(21) Fan, Q. L.; Zhou, Y.; Lu, X. M.; Hou, X. Y.; Huang, Wei. *Macromolecules* **2005**, *38*, 2927–2936.

(22) Silverman, B. D. *J. Mol. Evol.* **2005**, *60*, 354–364.